FRI-1.417-2-MEMBT-06

MODERN METHODS FOR MEASURING TEMPERATURE, STRESSES, AND STRAINS IN THE FIELD OF MICRO- AND NANOTECHNOLOGIES[7]

Emil Yankov, Chief Assist. Prof., PhD
Department of Material Science and Technology,
University of Ruse "A. Kanchev", Bulgaria
Tel.: 086-888-205
E-mail: eyankov@uni-ruse.bg

Maria P. Nikolova, Chief Assist. Prof., PhD
Department of Material Science and Technology,
University of Ruse "A. Kanchev", Bulgaria
Tel.: 086-888-306
E-mail: mpnikolova@uni-ruse.bg

Vanya Zaharieva, Chief Assist. Prof., PhD
Department of Material Science and Technology,
University of Ruse "A. Kanchev", Bulgaria
Tel.: 086-888-306
E-mail: vzaharieva@uni-ruse.bg

Abstract: *In recent years the stress and strain measurements have been implemented by laser-scanning systems and high-speed cameras monitoring the movements of pre-defined meshes. One of the crucial issues of these methods is the identification of the place of the necking region, that is usually accompanied by heat generation. In order to resolve this problem, specialized cameras enabling image taking in real time for processes such as deformation, heat treatment or model building with 3D printers are needed. In the particular study, the possibility of using a thermal imaging and infrared camera for separating the elastic from plastic zone during deformation and taking account of the sliding lines with the increase of load is demonstrated. This modern approach allows setting the occurrence of the necking region. On the other hand, during the building of the 3D models, the materials used are heated or melted and then they cool down that leads to the appearance of stresses and changes in dimensions thereafter. The stress occurrence is accompanied by residual temperature dissipations that could be registered by high technology thermal imaging cameras.*

Keywords: *Thermal cameras, Thermal imaging, Thermal analysis, Stress, Stress and strain deformation, Local stress, 3D Print, CAD 3D Model, Heat treatment, Temperature dissipations.*

INTRODUCTION

Nowadays, the commonest method for material testing – uniaxial tensile test, has been further developed and improved by different approaches in order to obtain more precise examinations of the deformed area of the samples. Digital electronic strain-gauge transmitters, laser- and optical systems, high-speed cameras, etc., could do this, for example. With the assistance of these methods, a more comprehensive picture of the plastic behavior of the materials during the loading process is obtained. Additionally, higher reliability for the mechanical properties and material behavior until the point of the critical loading is ensured. Such non-standard methods are applied during compression, bending, torsion or fatigue rests [1-3] complementing the standard methods of material testing [4-6]. The information obtained contributes not only to the developments in deformation processes' theory but it also enables an adequate simulation of the technological processes that unavoidable give new impetus to the development of the modern industry (INDUSTRY 4.0).

[7] Докладът е представен на пленарната сесия на 28 октомври 2017 на английски език. Заглавието на български език: СЪВРЕМЕННИ МЕТОДИ ЗА ИЗМЕРВАНЕ НА ТЕМПЕРАТУРА, НАПРЕЖЕНИЯ И ДЕФОРМАЦИИ В ОБЛАСТТА НА МИКРО- И НАНОТЕХНОЛОГИИТЕ

The infrared thermal cameras have been increasingly used for the examinations of the plastic deformation processes over the past few decades. They are suitable for defining the thermal field generated because of the transformation of a part of the mechanical energy into heat [8 - 10].

Biaxial hydraulic bulging tests of sheet metals have long been carried out in the laboratory for plastic deformation in the Department of Material Science and Technology of University of Ruse "A. Kanchev" [11, 12]. The information from the uniaxial tensile test concerning the anisotropy of the material is usually exploited for the data processing of the biaxial bulging test results. In the particular study, the method of passive infrared thermography was used to obtain greater clarification of the deformation processes and the preliminary results of the uniaxial tensile test of sheet steel samples were presented.

The infrared thermography method was also implemented for examining the heat fields arising during the 3D printing processes practiced in the Foundry Lab of the University [13]. This approach may impose the application of this method in the micro- and nanotechnology (MNT) area. It is common knowledge that the production of a qualitative printed part depends on many and various factors related to the thermophysical properties of the source material, the process parameters, the geometry of the object and the thermal conditions. The influence and interaction of the variety of factors are still not fully exploited which does not make it possible to minimize the occurrence of the defects and to guarantee consistently good quality. As known, the thermal conditions in which a certain printed part is produced play the key role in defects' formation. For example, the typical defects for the most frequently used materials - ABS and PLA, are the warping of the bottom part and separation of the layers in the form of external cracks. They arise from the non-simultaneous shrinkage of the adjacent layers due to the differences in their temperatures. The outside evidence for the warping is the separation of the peripheral zones of the basis from the table during the course of its production. To prevent the incoming defects, various working methods could be taken to increase mainly the adhesion of the material to the table. These are exploiting glass tables, coatings, glues, adding further elements acting like "steps" or suspending surfaces, etc. (Fig. 1) [14 - 16]. Such measures may lead to a positive effect only in some specific cases because they do not focus on the causes for the deformation occurrence on the base of the part. The more effective measures account the temperature influence and maintain a constant temperature of the working table and the surrounding environment by using temperature controlled working chamber. Consequently, the temperature gradients in the material during the printing process decrease resulting in a more even distribution of stresses and, therefore, less risk of undesirable deformations.

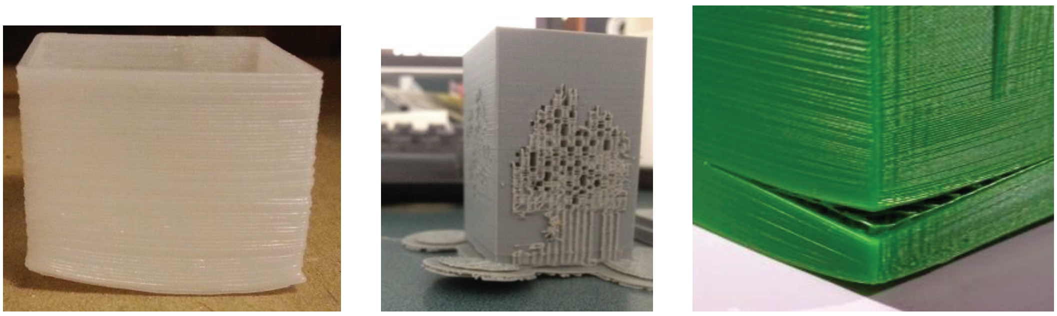

Fig. 1. *3D printed models indicating different problems occurring during the building process*

For monitoring the temperatures during the part production, thermocouples are usually used. Even employing a set of thermocouples positioned in certain points of the equipment so as to gather complete information of the thermal field, it is impossible to gain an adequate picture of the changing thermal profile of the product. The lack of such profile limits the possibilities for optimal modification of the part configuration and the process parameters. The latter has a determinative effect on the reliable and effective reduction of the defects in the products.

Using thermal cameras, thermographic images of the printed parts are acquired in real time. These images give a full overview of the thermal process during the printing process. The data collected from the set of thermographic images could be used for assessment of the degree of non-uniformity of the thermal field that leads to stresses and deformations occurring in the printed part.

MATERIALS AND EXPERIMENTAL PROCEDURES

One and the same thermal camera was used to examine the processes of uniaxial tensile test and 3D printing. Different models of such cameras were marketed. The cameras had an extended range of options that are appropriate for different areas under study. In the selection of the camera, the main requirements were as follow: an appropriate thermal interval ensuring correct image acquisition, high-temperature sensibility, high rate of capture and mobility. For that reason, the SEEK Thermal Compact Pro was chosen [17]. Its main characteristics were: temperature range from 0 up to 330 °C which was sufficient to enable the accuracy of the examined processes, the largest size of the thermal sensor being marketed - 320x240 pixel, thermal response below 70 mK with a spectral range of 7.5÷14 μm and capturing rate of 15 frames per second. In the capturing regime, the monitoring and registration of the maximum temperature at the surface of the sample and in the room were specified.

Table 1

Sample	Chemical composition									
	C	Si	Mn	Ni	S	P	Cr	Cu	As	Fe
Without coating	0.18	0.04	0.4	0.3	0.04	0.035	0.1	0.2	0.05	Bal.
With a Ni coating	0.02	0.018	0.42	0.17	0.008	0.021	0.033	0.08	0.011	Bal.

The static uniaxial tensile tests were performed on a universal testing machine Instron-3384 (Fig. 2 a). For the experiment sheet of low-carbon steel with chemical composition shown in Table 1 without coating and thickness of $t_o = 0.6$ mm and a coated with Ni sheet steel with a thickness of $t_o = 0.5$ mm were used. The specimens used for the tensile tests were cut on the base of standard ISO 6892-1:2009 (6 samples of each) (Fig. 2 c). The sheet samples were with the following dimensions: $L_o = 50$ mm, $L_c = 90$ mm, $L_t = 145$ mm and $b_0 = 20 \pm 1$ mm. For the purpose of the testing method, a constant strain rate of 10 mm/min was applied at ambient temperature.

The thermal camera was equipped with a mobile device and workable software Seek Thermal v.2.1.1.3. The set was adjusted in position to the front of the thermal chamber of the testing machine by a stalk (Fig. 2 a and b). The camera focused on the examined area of the sample so to capture the thermal fields in real time. The camera and machine synchronization were done by joining their software.

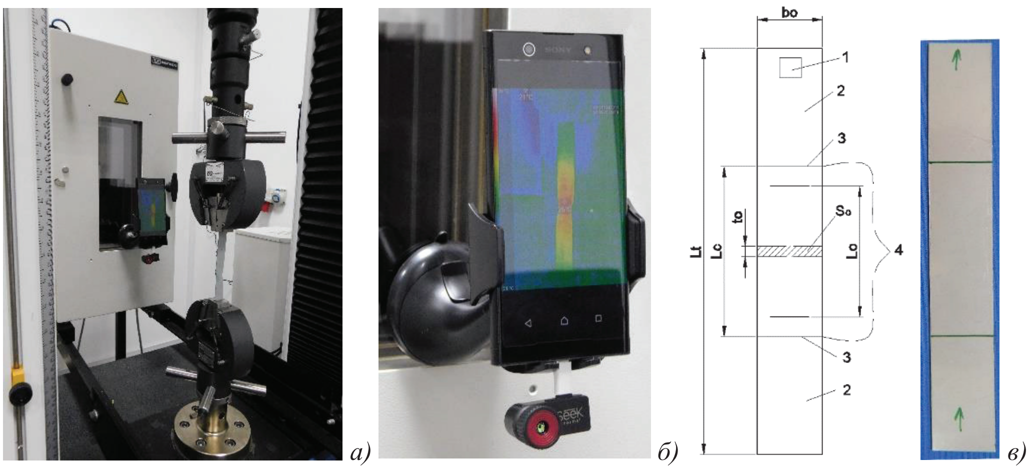

Fig. 2. *Tensile test equipment and samples: a) universal testing machine; b) SEEK Thermal Compact Pro camera together with the screen and clamp; c) test sample for the uniaxial tensile test (ISO-6892-1:2016).*

The thermographic examination of the 3D printing process was implemented by using Velleman K8200 (Fig. 3 a) printer. The thermal camera for imaging the different stages of the printing process was stationary mounted to a suitable place on the printer basis (Fig. 3 b). The camera positioning was dependent on the location of the zones where the warping or layers' separation were expected.

For the purpose of the investigation, a digital model by the CAD system Autodesk Inventor was designed (Fig. 3 c). The model geometry formed areas different in sizes and cross-sections that allowed the occurrence of warping and unsticking of the model from the table. One of the sidewalls of the model was designed at an angle of 30° inclination in order to stimulate the layers' separation. The height of the model (15 mm) was chosen based on the data of gathered experience for the occurrence of the layers' separation effect. For the building of the model, PLA material with grey-metallic color and diameter of 2.9 mm was utilized. The process parameters used were as follow honeycomb filling, 0.2 mm layer thickness, 30% filling density, printing temperature of 200 °C, the temperature of the working table equal to 55 °C. The software used for designing the 3D printing program was Repetier V2.0.1.

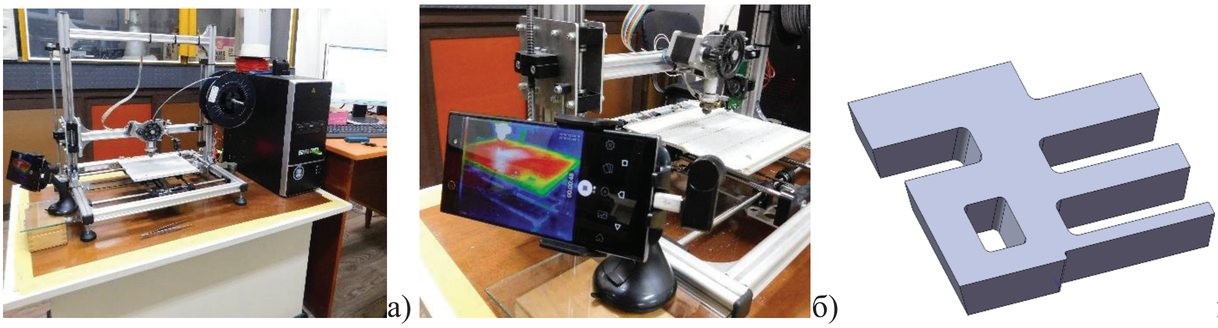

a) б) в)

Fig. 3. *3D printing: a) Velleman K8200 printer, b) SEEK Thermal Compact Pro camera together with the screen and clamp, c) model of the printed part*

RESULTS AND DISCUSSIONS

With the assistance of the thermal camera, several datasets of thermographs were captured during the uniaxial tensile tests of the uncoated samples. The ambient temperature during the tests was equal to 21 °C. The capturing process included the whole test from the beginning to the end where the rupture occurred. The comparative analysis of the real-time videos showed the same picture of all tested samples. Fig. 4 displays four thermographs corresponding to different moments of the deformation process of one of the samples. The same images are matched with the extension-strength diagram and shown in Fig. 5.

The detailed data analysis of the videos taken during the initial stages of the test where the elastic region of deformation is found gives rise to some observations. First, it was noted that there were fluctuations in the temperatures of different surface zones ranging from 19 °C to 25 °C. Moreover, the surface radiation was not homogenous and showed spot character – individual micro-regions corresponding to bright yellow micro-spots in the images emitted the heat. During the elastic deformation, the quantity of the bright-yellow regions varied without a trend of increasing with the increase of load. During the elastic deformation, the camera captured several moments of brighter lightening of the samples suggesting pulse radiation of heat from the surface. There are some literature data concerning temperature fluctuations in the elastic region of tensile tested samples. In this region, most of the researchers found slight temperature decrease of about 0.5 °C at the surface [12-15]. The thermo-mechanical effects in the elastic area were not studied in details probably because of the raising interest toward the materials' behavior in the plastic region. The characteristics of the thermographs should be linked to the specific mechanism of deformation of the polycrystalline materials when loaded within the elastic region.

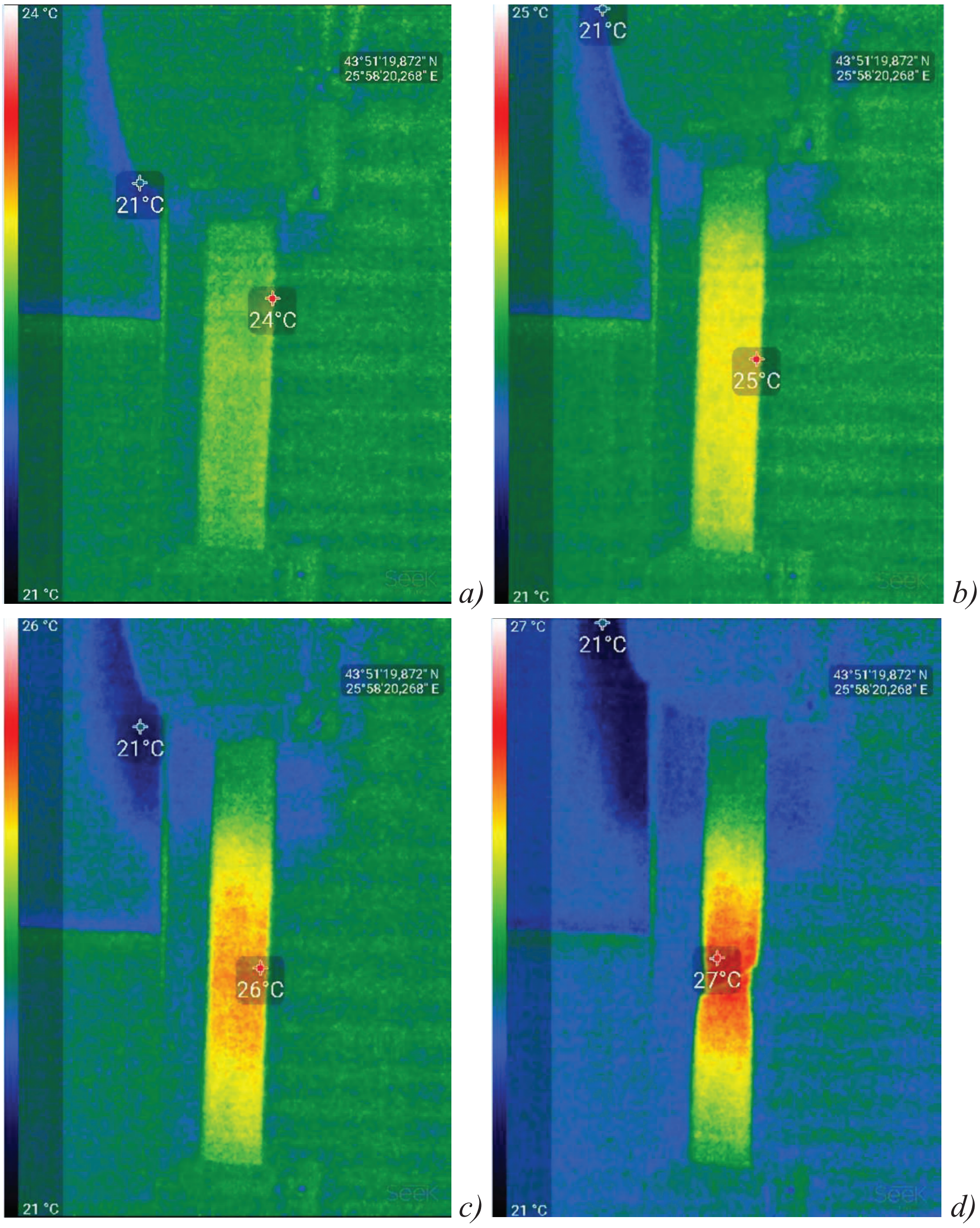

Fig. 4 *Thermographic images of the uncoated sample of low carbon steel during the uniaxial tensile test.*

The heat radiation emitted from discrete micro-areas of the samples came from the plastic deformations occurring in restricted micro-zones. It may be presumed that the repeated pulse radiations of heat in the elastic region arose from the collective effect of the simultaneous and instantaneous run of numerous micro-plastic deformations. However, they are so small that the standard methods of tensile testing could not detect the plastic component in the elastic area. The intervals between the pulse radiations of heat could be explained by the necessary preparation time, nucleation and growth of the new plastically deformed micro-zones. These processes are similar to the nucleation and growth process during the phase transformations. A reduction in the fluctuations of the bright spots characterized the transition in the plastic region and emphasized on maximizing the temperature in the middle zone to an average of 24 °C. When reaching and increasing the temperature above 24 °C at the surface, the material entered in the plastic area (Fig. 4 a). In this area, the temperature fluctuations decreased while the plastic deformation increased. The image showed highly pronounced lighter areas in which red colored micro-zones with higher temperature were distinguished (Fig. 4 b). This effect could probably be attributed to micro-deformation with greater intensity in some micro-areas. The regions near the jaws displayed lower temperature due to the intensive cooling in the contact areas.

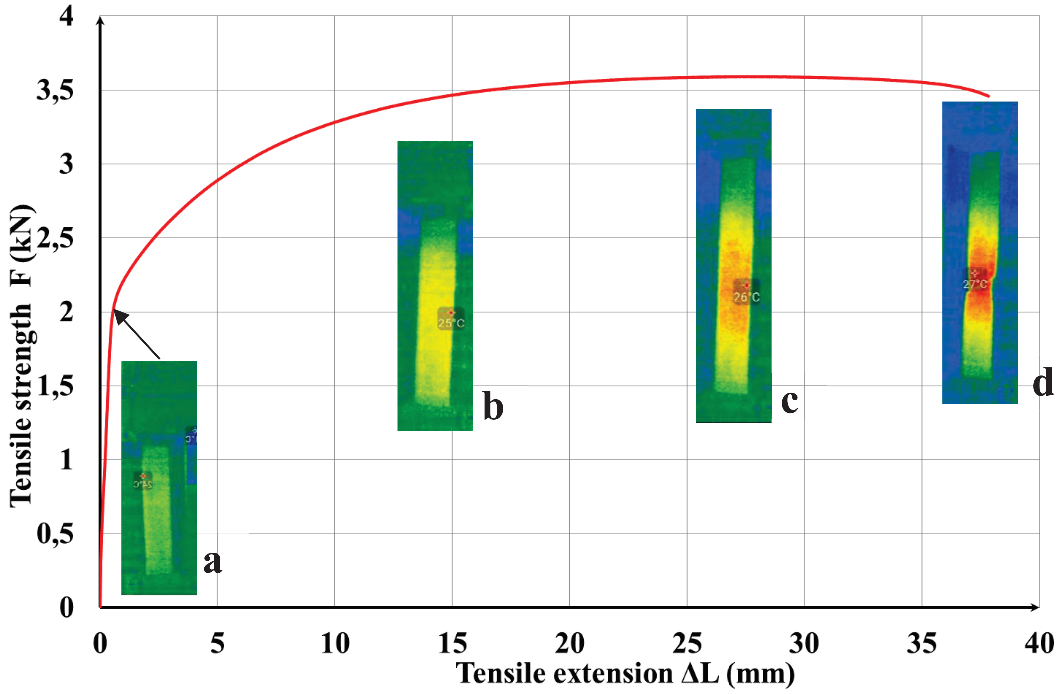

Fig. 5. *Tensile extension-strength diagram of the uncoated low-carbon steel*

With the increase in load, while bringing closer to the maximal strength of the material, intensive heat radiation zone was formed localizing the necking region (Fig. 4 c). It is worth noticing that the formation of this zone proceeded the start of neck initiation. Therefore, the gathered information could be used for monitoring and influencing the zones with exhausted plasticity allowing reaching higher degrees of uniform plastic deformation of sheet metal materials.

In the final stage of loading, the heat radiation was concentrated in the necking region. This was an estimated effect since while decreasing the cross-section and the deformation volume, the internal trans-crystal movements and the accompanying wear increase the heat radiation of the necking zone (Fig. 4 d). In the breaking down zone, the temperature reached its maximum value.

In Fig. 5, the four images are matched with the tensile extension-strength diagram as their positions coincide with the respective areas of the test.

The tensile test results from the second set of samples with sandwich Ni-coating are shown in Fig. 6 and 7. Fig. 6 displays four thermographs corresponding to selected moments from the deformation process of one of the samples. These were the initial stage of the plastic deformation (Fig. 6 a), the area of uniform plastic deformation (Fig. 6 b), the region of maximum loading (Fig. 6 c) and the moment of local rupture (Fig. 6 d). Compared to the first set of samples without coatings, less heat radiation could be seen because of the coating presence. This fact demonstrates the differences in the properties of the substrate and the coating.

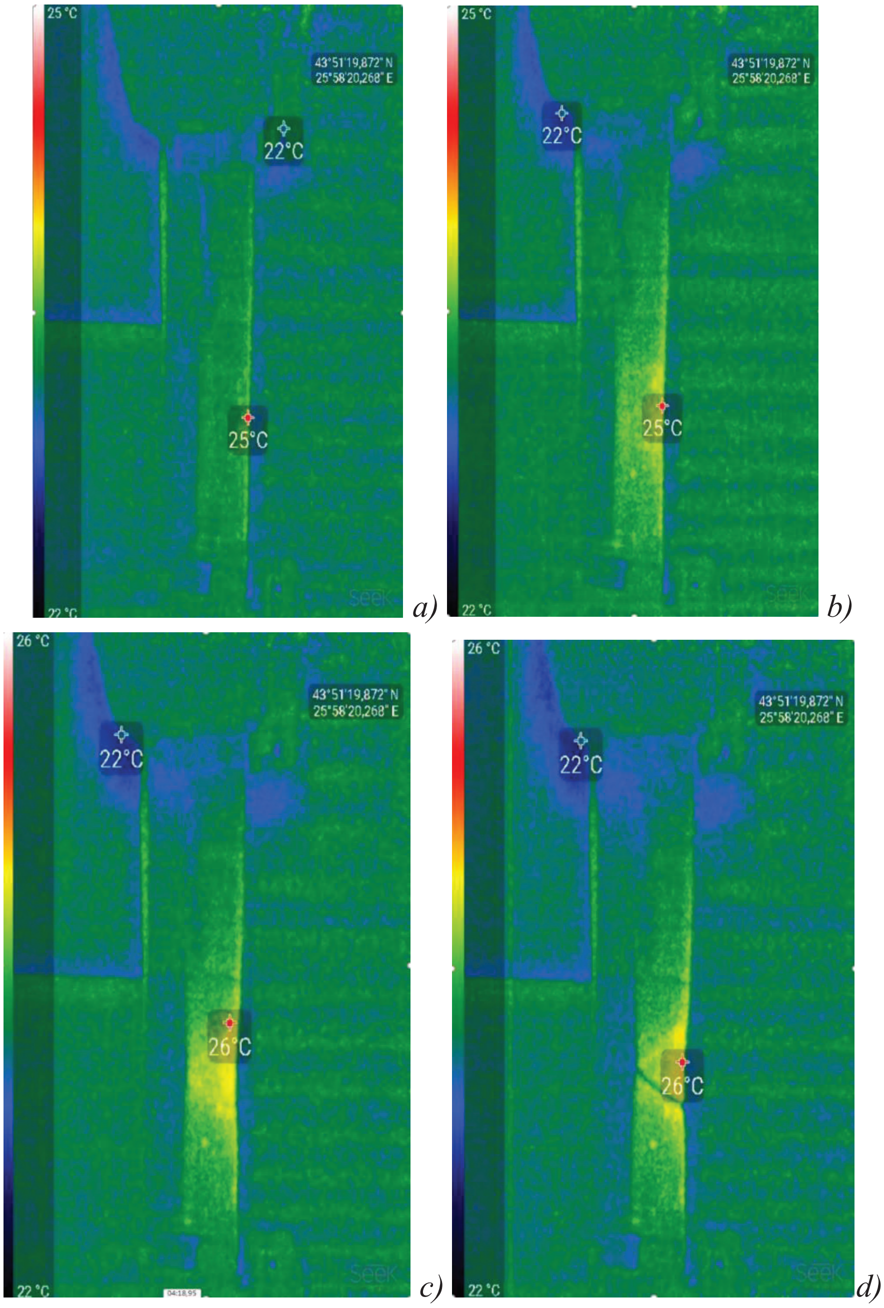

Fig. 6. *Therographic images of the Ni-coated sample of low carbon steel during the uniaxial tensile test.*

In the elastic region, the tracking video registered similar but less pronounced deformation specificities. The transition area from elastic to plastic deformation was hard to be identified (Fig. 6 a). In the area of uniform plastic deformation, the heat radiation was concentrated in the highly deformed region. When the maximum loading was reached, pulse bright lighting was detected after which the necking region took shape (Fig. 6 b). The zone with maximum temperature appeared to have clearer wedged-shape form. The regions of maximum trans-crystal movements outlined in the necking zone (Fig. 6c). The contours of the wedged-shape region where the heat radiation was the highest were the breaking place of the material.

The four images (Fig. 6) matched with the tensile extension-strength diagram are shown in Fig. 7.

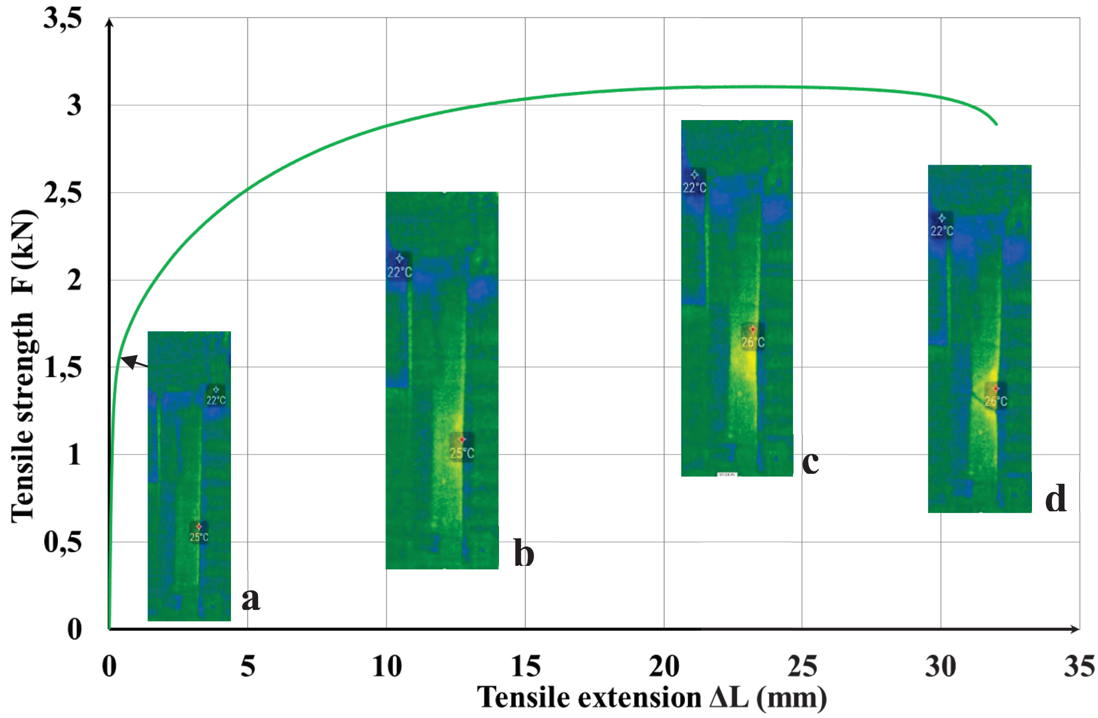

***Fig.** 7. Tensile extension-strength diagram of the Ni-coated steel.*

The presence of coating affected the tensile extension-strength diagrams by reducing the tensile yield strength and increasing the maximum tensile strength. The maximum tensile strength for the uncoated low-carbon steel went up to 300 MPa at a true strain of 33 % while the true strain of 33 % for the Ni-coated samples had been reached at 565.15 MPa (Fig. 8). The maximum elongation at maximum load of F_{max} = 3.59 kN was equal to ΔL = 27 mm for the low-carbon steel (Fig. 5), while the former for the coated one amounted to ΔL = 27 mm at a load of F_{max} = 3.11 kN (Fig. 7).

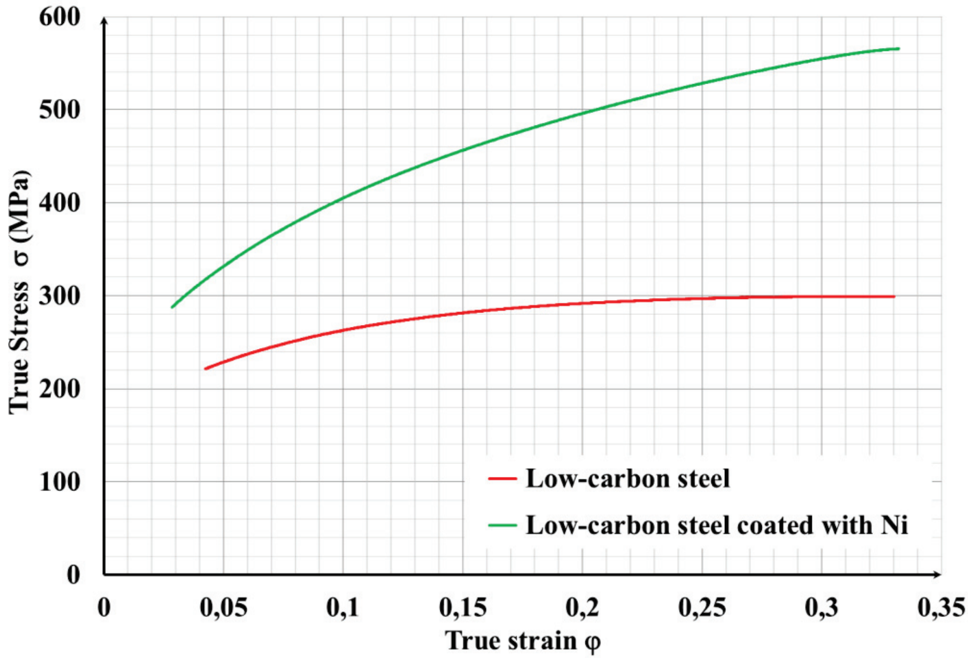

***Fig. 8**. True stress-strain diagram of both tested samples*

The interesting facts registered in the elastic region and elastic-plastic transition are worthwhile to be examined. This would allow using a convenient way to determine the elastic-plastic transition especially for materials with a smooth transition in this area. This effect makes it difficult to determine the respective stress in the diagram with sufficient precision. Additionally, the possibility to establish the moment and the place of rupture before the necking region formation is of particular scientific and practical importance. When testing coated samples, a more careful approach and refining the methodology are needed.

The second part of the examination focuses on the thermal fields in the working area of the 3D printing process. Building the first layer of the model, the working temperature of the table was equal to 70 °C so to decrease the thermal gradient between the table and the extruded material and to enable good adhesion between them. For the rest of the layers, the temperature setting of the table was 55°C. The initial thermal field of the working table before the printing is shown in Fig. 9. As is seen, the thermal field was non-homogenous – the temperature in the central zone was about 70 °C while in the periphery the temperature decreased continuously to around 50 °C. This creates the conditions of unequal adhesion of the material to the surface of the table. During the first layer formation, when the contours of the model were printed (Fig. 10 a), the additional heat was put to the liquidized material (Fig.10 b). As expected, the highest was the temperature increase for the 15 mm width zone (the brighter spot in the image) where the comb-like region of the model appeared. Following the different weight of the zones with 5, 10 and 15 mm width, the cooling proceeded at different rates. The different heat radiation intensity of the tree zones clearly demonstrated this effect (Fig. 10 b). The same effect was observed when a growing number of layers were printed (Fig. 10 c). Each layer formation is accompanied by alternating heating of already printed layers and their cooling down in the air. These processes lead to expansion and shrinkage of the material. Under the cooling influence, the three zones with 5, 10 and 15 mm width shrank freely in a cross pattern. As regards width, the maximum shrinking was in the 15 mm zone. Increasing the numbers of layers shrinkage difficulties were starting to show because of the layers' linkage and the different temperature of the adjacent layers. Due to the shrinkage difficulties, thermal stresses arose in the material. The edges of the three zones with different width showed unequal cooling rates. After printing the sixth layer, the residual stresses overcame the adhesion strength at the end of the 15 mm zone and lead to deformation and separation of the model from the table (Fig. 10 d).

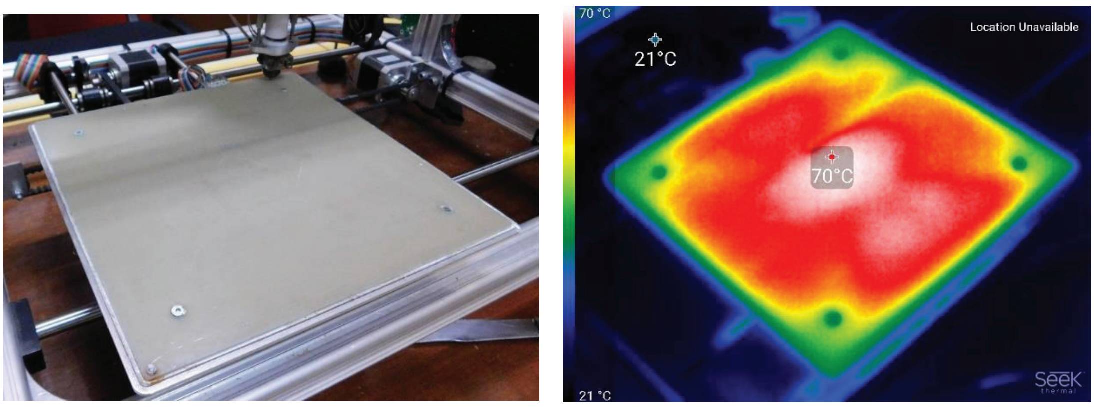

Fig. 9. *The working table and its thermal field immediately prior to the 3D printing process*

After printing the 12th layer (Fig. 10 e), the degree of deformation was so high as to impede the 3D printing process of the model because of the blocked movements of the printer head.

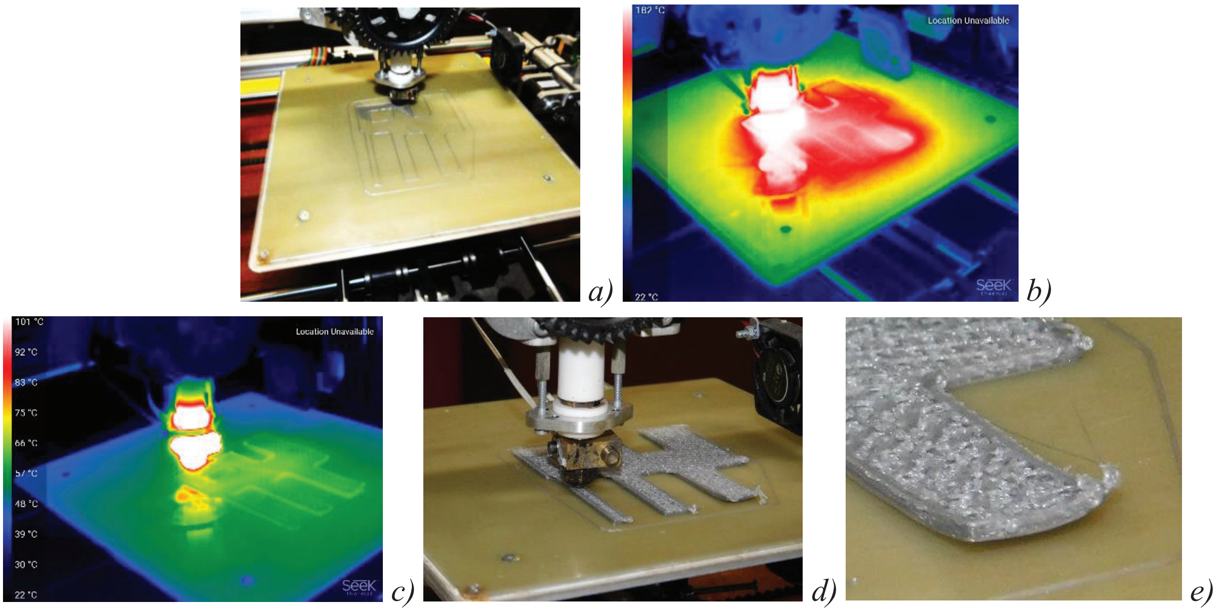

Fig. 10. *Different stages of the layer-by-layer printing of the 3D model a) building of the first layer; b) a thermograph of the initial stages of the model printing; c) a thermograph after building the sixth layer; d) recurrence of a model separation after the tenth layer printing; e) separation of the model after printing twelve layers.*

The small thickness of the model hindered the acquisition of clear thermal gradient images in the height. This gradient should be responsible for the stress accumulation and possible layers' separation in the model.

The preliminary studies in the 3D printing area show that with the assistance of thermography useful information about the thermal fields in the working area is obtained. The proposed thermal method immediately ignores the assumption that the working table is homogeneously heated. Only one thermocouple maintained the table temperature. The uneven temperature distribution depending on the model configuration allows identifying the causes for printing defect occurrence. The monitoring of the thermal field during printing enables a prompt respond and implementation of corrections during the 3D printing process.

CONCLUSIONS

1. By using the infrared thermography method during the uniaxial tensile test, a complete information concerning the mechanism of the deformation process, the place of the rupture area and the moment of initiation of the necking could be obtained.
2. The tensile tests results and the captured by infrared thermography images will be useful for comparison purposes and analysis of the differences between the uniaxial tensile test and biaxial hydraulic bulging of sheet metals and alloys.
3. The 3D printing process examination by infrared thermography permits adequate analysis concerning the reasons for the occurrence of deformations in the base of the model, loss of adhesion between the model and the table, layers' separation, etc.
4. The experimental results from the thermal fields will provide useful information for optimising the building strategy of models during the 3D printing processes.
5. The thermal analysis method could be used for the assessment of plausibility and precision of simulation of 3D printing processes.

REFERENCES

[1] Korsunsky, A. M., Bemporad, E., Sebastiani, M., Hofmann, F., Saraansh D., Measurement and Interpretation of Residual Stress at the Micro-Scale, *International Journal of Modern Physics B,* Vol. 24, Nos. 1 & 2 (2010), pp. 1–9, DOI: 10.1142/S0217979210063910.

[2] Hamdia, P., Steada, D., Elmob, D. (2015). *Journal of Rock Mechanics and Geotechnical Engineering*, Volume 7, Issue 6, December 2015, pp 609-625, https://doi.org/10.1016/j.jrmge.2015.07.005;

[3] Usamentiaga, R., Venegas, P., Guerediaga, J., Vega, L., Molleda, J. and Bulnes, F. (2013), Infrared Thermography for Temperature Measurement and Non-Destructive Testing, *Sensors 2014*, 14 (7), pp 12305-12348; doi:10.3390/s140712305;

[4] Ming, H., Ruolin, Z., Zhang, Z., Wang J., Han, En-Hou., Ke, W., Su, M. (2016). Microstructure, Local Mechanical Properties and Stress Corrosion Cracking Susceptibility of an SA508-52M-316LN Safe-end Dissimilar Metal Weld Joint by GTAW, *Materials Science and Engineering A 669* May 2016, pp. 279-290, DOI: 10.1016/j.msea.2016.05.101;

[5] Dave, S. The Development of Strain Correlation for Deformation Analysis at the Grain Scale, *4th Year project, Department of Engineering Science*, University of Oxford (2009);

[6] Янков Е., Николова, М., Захариева, В., Господинов.Д., (2014), Механични, структурни и фазови изменения при едномерен опън на листови материали, Машиностроене и машинознание, 2014, брой Книга 2, №21, стр. 24-29, ISSN 1312-8612;

[7] Yankov, E., Nikolova, M., Zaharieva, V. (2015), Mechanical and Structural Changes of Austenitic Sheet Metal Alloy during Biaxial Tensile Straining by Hydraulic Bulging. *UR&US'2015*, Ruse, Vol. 54, Issue 2, 2015, pp. 89-98, ISBN ISSN 1311-3321;

[8] Stewart, M.; Webster, J.; Schaefer, A.; Cook, N.; Scott, S. Infrared thermography as a non-invasive tool to study animal welfare. Anim. Welf. 2005, 14, 319–325;

[9] Meola, C.; Carlomagno, G.M. (2004), Recent advances in the use of infrared thermography, *Meas. Sci. Technol. 2004*, 15, R27;

[10] Luong, M.P. (1998), Fatigue limit evaluation of metals using an infrared thermographic technique. *Mech. Mater*. 1998, Vol. 28, pp. 155–163;

[11] E. Yankov, „Sheet materials testing using biaxial hydraulic bulge test“, Dissertation, Ruse, p. 112 (2014);

[12] E. Yankov, M. Nikolova, MATEC web of Conferences, CoSME'16, 94, DOI: 10.1051/matecconf/20179402017 (2017);

[13] 2014 ПРОЕКТ 2014-ФМТ-02, ФНИ на РУ „А. Кънчев” на тема „Разработване на интегрирана технологична верига за прецизно вакуумно леене по стопяеми модели изградени чрез бързо прототипиране”;

[14] https://www.google.bg/search?q=curling+3d+printing&source=lnms&tbm=isch&sa=X&ved=0ahUKEwjmmNzR0o7XAhURS5oKHWhdDYcQ_AUICigB&biw=664&bih=710#imgrc=NmT330rhHkmUEM;

[15] https://www.google.bg/search?q=curling+3d+printing&source=lnms&tbm=isch&sa=X&ved=0ahUKEwjmmNzR0o7XAhURS5oKHWhdDYcQ_AUICigB&biw=664&bih=710#imgdii=XDTlKU360KAlRM:&imgrc=V2oUuHI416HnSM;

[16] https://www.google.bg/search?q=curling+3d+printing&source=lnms&tbm=isch&sa=X&ved=0ahUKEwjmmNzR0o7XAhURS5oKHWhdDYcQ_AUICigB&biw=664&bih=710#imgrc=gHm_D_fKLtvnZM;

[17] https://www.brannik.bg/ekipirovka/ovni-kameri/termalna-kamera-seek-thermal-compactpro-za-android/.